JOURNAL OF AIRCRAFT
Vol. 29, No. 5, Sept.–Oct. 1992

Application of Computational Fluid Dynamics to Sonic Boom Near- and Mid-Field Prediction

Samson H. Cheung,* Thomas A. Edwards,† and Scott L. Lawrence‡
NASA Ames Research Center, Moffett Field, California 94035

A technique combining a quasilinear extrapolation theory and a three-dimensional parabolized Navier-Stokes (PNS) code has been used to calculate the supersonic overpressure from three different geometries at near- and mid-fields. Wind-tunnel data is used for code validation. Comparison of the computed results with different grid refinements, and different extrapolation distances, are shown in this article. It is observed that a large number of grid points is needed to resolve the tail shock/expansion fan interaction. Therefore, an adaptive grid approach is employed to calculate the flowfield. The effects of a thin, attached boundary layer and the sting of the wind-tunnel model to the sonic boom have also been studied in this article. The agreement between the results and the wind-tunnel data confirms that this technique can be applied to the problem of sonic-boom prediction.

Introduction

THE sonic-boom disturbance produced by current commercial supersonic transports is too disruptive for routine overland flight. In this article, the term sonic boom refers to the pressure disturbances at a designated distance from the aircraft. Since sonic booms are environmentally objectionable, commercial supersonic flight over land is currently banned throughout most of the world. It is known that by properly distributing the airplane lift, the pressure-pulse associated with the sonic boom can be alleviated.[1] In the design cycle of low-boom airplanes, sonic-boom prediction must be accurate.

Different types of equations are needed for sonic-boom prediction in the near-, mid- and far-fields. This is illustrated by the sketch in Fig. 1. The near-field includes the flow relatively close to the body, normally within a few characteristic lengths. In general, the detailed solution of the near-field flow is of interest in problems of determining the surface pressure distribution for the calculation of forces on the body. However, when complex near-field solution techniques are employed to calculate the flow further from the body, such as for prediction of the sonic boom, the numerical calculations become increasingly inaccurate, time-consuming, and often unstable. The mid-field includes the flow from a few to perhaps a hundred characteristic lengths. Here the flow is entirely supersonic and can be considered inviscid. Shocks are sufficiently weak that the flow can be considered homentropic, however, the nonlinear behavior of the compressions and expansions produced by particular features of the body cannot be neglected. The far-field is defined to be the flow far from the body, typically beyond several hundred to a thousand characteristic lengths. All intermediate shocks have decayed or coalesced with either front or rear shock, and the overpressure signature has evolved into the classical *N*-wave.

For more than two decades, many researchers have studied the nature of sonic boom.[1-3] Wind-tunnel experiments from simple geometries to complex aircraft configurations were conducted to determine the validity of sonic-boom-prediction theory and to seek low-boom configurations.[4,5] The basic sonic-boom theory originated in a classic paper by Whitham.[6] Whitham's theory is a modification of linearized theory that permits the coalescence of disturbances into shocks for smooth bodies of revolution. Basic to its application is the formulation of the *F*-function, which is related to the equivalent area distribution of the aircraft. For isentropic axisymmetric flow, the pressure disturbances at large distances from the aircraft can be expressed in terms of the *F*-function. An alternate formulation of the *F*-function that was derived by Lighthill[7] for nonsmooth bodies was shown to be better for sonic-boom prediction for smooth and nonsmooth projectile shapes. Later, Walkden showed that the Whitham theory could be applied to winged bodies.[8]

There are two main techniques for reducing sonic boom: 1) aerodynamic minimization, and 2) exotic configurations.[9] The former technique involves the calculation of an optimal flight altitude such that the N-wave is minimized. The latter involves design of the aircraft so that the mid-field pressure disturbance, e.g., a finite-rise shock, is retained to the ground before it turns into a noisy N-wave. Recently, researchers have concentrated on the second technique. The *F*-function theory is used as a sonic-boom-prediction tool in the iterative loop of the low-boom aircraft design[10] and wind-tunnel investigation.[11] However, this linear theory fails in highly non-

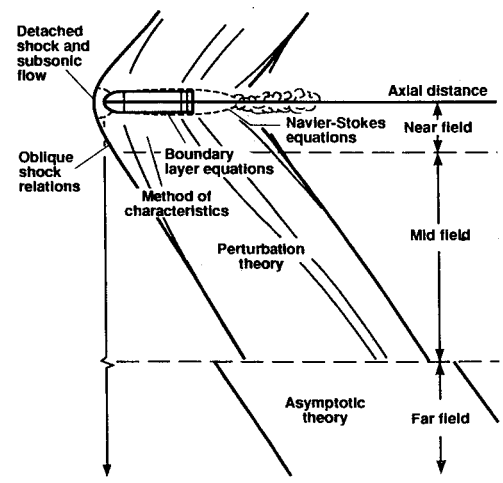

Fig. 1 Flow around a supersonic projectile showing the near-, mid-, and far-fields.

Received Jan. 24, 1991; revision received Sept. 26, 1991, accepted for publication Oct. 14, 1991.

*Research Scientist, MCAT Institute. Member AIAA.
†Assistant Chief, Applied Computational Fluids Branch. Senior Member AIAA.
‡Research Scientist. Member AIAA.

linear flow, such as the flow at angle-of-attack, at higher Mach numbers (between 3 and 5), and flows involving caustics.

The present study combines the efforts of computational fluid dynamics (CFD) and Whitham's quasilinear theory to the problem of sonic-boom prediction. A three-dimensional parabolized Navier-Stokes (PNS) code is applied to three sonic-boom model problems. Three different approaches are taken to obtain the overpressure signal at mid- and far-field from a near-field CFD solution. The comparisons of wind-tunnel data and the results obtained by the three approaches will be presented. These comparisons give a good idea of how well the combination of CFD and the quasilinear theory perform in sonic-boom prediction, and the role CFD could play in sonic-boom prediction and minimization. The three wind-tunnel sonic-boom models in this paper are obtained from Refs. 4 and 5.

Numerical Scheme

The PNS equations have been used for the efficient prediction of three-dimensional, steady, supersonic, viscous flowfields. The efficiency is achieved in both computer time, and memory requirement, because the equations can be solved using a space-marching technique rather than time-relaxation. Furthermore, since the PNS equations are valid in both the inviscid and viscous regions of the flowfield, the interaction between these regions of the flowfield is automatically accounted for. Recent design studies for high-speed civil transports have focused on Mach 2–3.2 at cruise.[12] Since the design process is iterative, a fast prediction method is needed, therefore, the PNS approach is used in predicting the pressure disturbances in this study.

Nevertheless, there are certain limitations associated with parabolization of the full Navier-Stokes equations. The streamwise derivatives of the viscous terms are neglected. The inviscid region of the flow must be supersonic and the streamwise velocity component must be positive everywhere. The last requirement excludes streamwise flow separation, but crossflow separation is permitted.

The computational code used in this study, called the UPS3D code,[13] integrates the PNS equations using an implicit, approximately factored, finite-volume algorithm where the crossflow inviscid fluxes are evaluated by Roe's flux-difference splitting scheme.[14] The upwind algorithm is used to improve the resolution of shock waves over that obtained with conventional central differencing schemes. The UPS3D code has been successfully applied to a number of hypersonic problems including flow past a circular cone[13] and turbulent flow past a generic all-body hypersonic vehicle.[15]

In addition to the capability of solving the PNS equations, the UPS3D code also calculates the inviscid flowfield by solving the PNS equations without the viscous terms. The code also features fully three-dimensional, bilateral, quadrilateral, and axisymmetric flow modeling capabilities.

F-Function Theory

A currently accepted method of obtaining a pressure signature from the *F*-function (based on an equivalent area distribution of the flying object) was first introduced by Whitham in 1952.[6] This quasilinear theory assumes isentropic axisymmetric flow and small pressure disturbances. The asymptotic form of the equations used in developing the sonic boom overpressure signature ($\Delta p/p_\infty$) is[6,8,16]

$$F(y) = \frac{1}{2\pi}\int_0^\infty \sqrt{\frac{2}{\beta R_{\text{vol}}(t)}}\, h\left[\frac{y-t}{\beta R_{\text{vol}}(t)}\right] \mathrm{d}S'_{\text{vol}}(t) + \frac{1}{2\pi}\int_0^\infty \sqrt{\frac{2}{\beta R_{\text{lift}}(t)}}\, h\left[\frac{y-t}{\beta R_{\text{lift}}(t)}\right] \mathrm{d}S'_{\text{lift}}(t) + \frac{1}{2\pi}\int_0^\infty \sqrt{\frac{2}{\beta R_{\text{int}}(t)}}\, h\left[\frac{y-t}{\beta R_{\text{int}}(t)}\right] \mathrm{d}S'_{\text{int}}(t) \tag{1}$$

$$\frac{\Delta p}{p_\infty} = \gamma M_\infty^2 F(y)/\sqrt{2\beta r_0} \tag{2}$$

$$x|_c = y + \beta r_0 - \kappa\sqrt{r_0}F(y) \tag{3}$$

where Δp is $(p_{\text{local}} - p_\infty)$, $\gamma = 1.4$ for air, M_∞ is the freestream Mach number, $\beta = \sqrt{M_\infty^2 - 1}$, $\kappa = (\gamma + 1)M_\infty^4/\sqrt{2}\beta^{3/2}$, R is the radius (or equivalent radius) of the flying object, S' is the derivative of the area distribution of the flying object, and h is the Heaviside unit step function.[6] Here, $y(x, r_0)$ constant is a characteristic curve, x is the streamwise distance, and r_0 is the distance normal to the flight axis. The first integral of Eq. (1) is associated to the volume of the flying object; the second integral is associated with the lift; and the third integral is associated with the interference lift for a winged body.[8]

Unfortunately, it is noticed that at higher freestream Mach numbers ($M_\infty > 2$) and/or higher lift coefficients (angle-of-attack), this theory disagrees with wind-tunnel data.[4] Figure 2 shows the discrepancy of the wind-tunnel data and the result of this quasilinear theory as lift coefficient increases. The case in Fig. 2 is one of the three test cases studied in this article; further results will be presented later.

Reference 16 described an *F*-function extrapolation method that extrapolated the pressure signature at r_0 to a further distance r_1. First, a pressure signature ($\Delta p/p_\infty$) at distance r_0, where the flowfield is assumed locally axisymmetric, is directly measured in the wind-tunnel; and the value of the *F*-function (at r_0) can be calculated from Eq. (2). Then y_t is defined as

$$y_t = x - \beta r_1 = y - \kappa\sqrt{r_1}F(y)$$

Since the pressure signal propagates at the local speed of sound, and each point of the signal advances according to its amplitude, the signal is distorted and the *F*-function becomes multivalued, as shown in Fig. 3. A new *F*-function at r_1 is

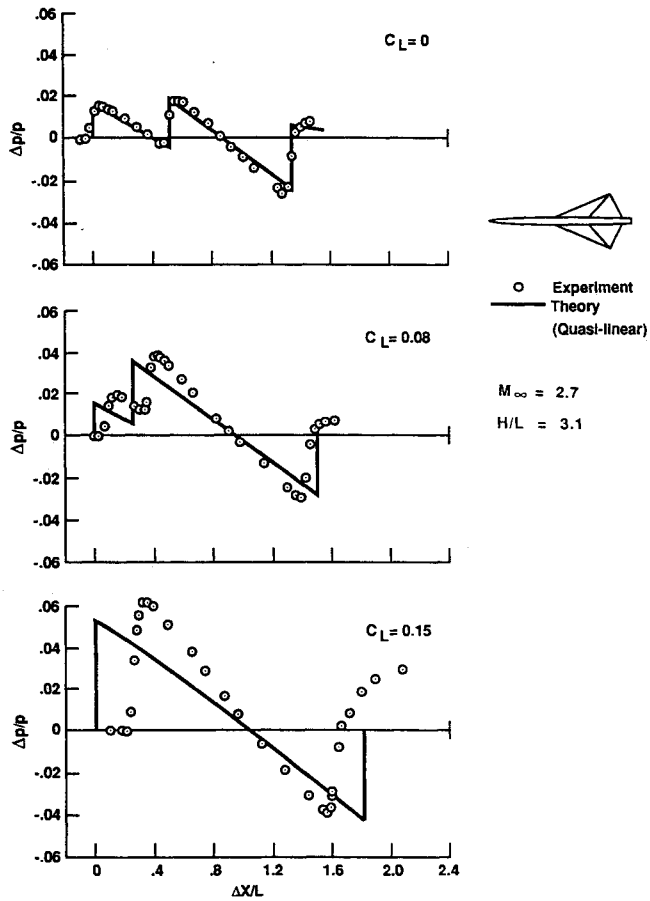

Fig. 2 Discrepancy of the quasilinear theory based on equivalent area distribution and wind-tunnel data as lift coefficient increases.

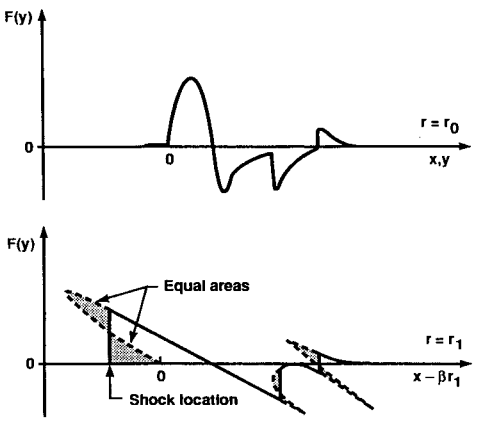

Fig. 3 Transposed F-function and the location of the shocks determined by the equal-area rule. The shaded areas are replaced by a discontinuity.

obtained by placing discontinuities (shocks) in such a way that the equal-area rule is satisfied (see Fig. 3). This new F-function gives the overpressure signature at r_1 by [using Eqs. (2) and (3)]:

$$\Delta p/p_\infty = \gamma M_\infty^2 F(y)/\sqrt{2\beta r_1} \qquad (4)$$
$$x|_c = y_t + \beta r_1$$

CFD Extrapolation Interface

The difference between sonic-boom predictions using Whitham's quasilinear theory and the wind-tunnel data at higher freestream Mach numbers and/or higher lift coefficients is generally attributed to the strong shocks that are generated in these regimes that have significant entropy production. These effects are neglected by the quasilinear theory.

In this article three approaches are exercised to predict the sonic boom at mid- and far-fields. First, the near-field three-dimensional solution is obtained by applying the CFD code to the flow immediately surrounding the body. The three approaches to propagating this disturbance to the mid- and fair-field are described as follows:

Approach 1) For nonlifting cases, the UPS3D code is modified so that it has an axisymmetric version (UPSYM) that provides a propagation capability that incorporates all nonlinear effects. At a distance downstream where the near-field three-dimensional solution is assumed axisymmetric, the UPSYM code is employed to advance the solution downstream to the desired distance.

Approach 2) For both lifting and nonlifting cases, the near-field three-dimensional solution provides the overpressure signal at a near distance r_0. By the technique described in the previous section (Eq. (4)), the sonic boom at further distance r_1 can be extrapolated from the near-field solution.

Approach 3) For lifting cases, the equivalent area distribution due to lift, is generated by the surface pressure coefficients calculated by the UPS3D code. The equivalent area distribution due to volume is calculated directly from the geometry of the flying object. Summing the two equivalent area distributions gives the total equivalent area distribution, that gives the F-function of the lifting body.[6–8] Then the sonic boom can be predicted by Eqs. (2) and (3).

Sonic-Boom Prediction

Three configurations, a cone-cylinder, a low-aspect-ratio rectangular wing, and a delta-wing body, were studied. These were simple geometries for which wind-tunnel data were available for comparison.

Model 1: Cone-Cylinder

The cone-cylinder shown in Fig. 4 had a cone angle of 6.48 deg.[5] In this test case the freestream Mach number was 1.68.

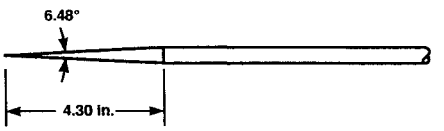

Fig. 4 Model 1: Cone-cylinder model.[5]

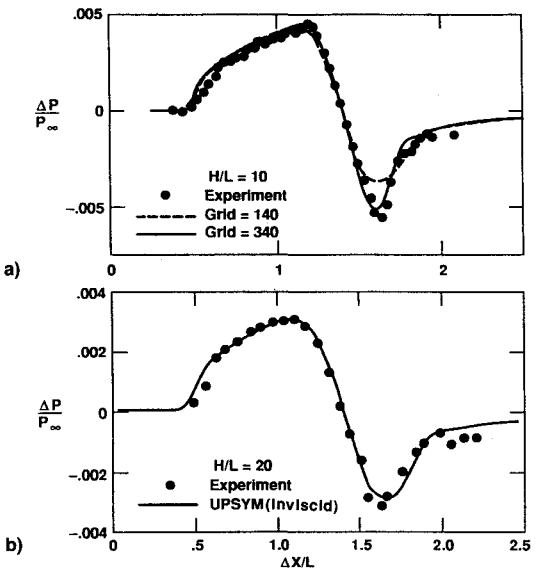

Fig. 5 a) Variation of predicted overpressure signal at 10 cone lengths with radial grid resolution. Model 1, $M_\infty = 1.68$. b) Overpressure signal at 20 cone lengths. Model 1, $M_\infty = 1.68$.

The experimental overpressure signature was measured at distances of 10 and 20 cone lengths ($H/L = 10$ and 20) from the cone. These calculations were performed at zero angle of attack ($\alpha = 0$).

The inviscid calculation (three-dimensional mode of UPS3D) of the near-field solution for the half-plane used a grid containing 21 grid lines in the circumferential direction and 140 in the normal (or radial) direction. This three-dimensional calculation was only carried from the nose to about $\frac{1}{10}$ of the cone length and was used as a starting solution for UPSYM on a grid containing 2 grid lines in the circumferential direction and 340 in the normal direction. The overpressure calculation was obtained at 10 and 20 cone lengths using the UPSYM code. In the streamwise direction, the marching code took a step-size of about 1% of the cone length. This UPSYM extrapolation required 4–6 min of central processing unit (cpu) time on the Cray-YMP to obtain the pressure signature at 10 cone lengths.

The overpressure predictions at 10 and 20 cone lengths shown in Figs. 5(a) and 5(b), respectively, confirm the propagation capabilities of the code. All the numerical solutions shown in this paper were shifted to align the computational and experimental signatures at $\Delta p/p_\infty = 0$ in the expansion region. The abscissa, $\Delta x/L$, is the shifted distance divided by the characteristic length. Figure 5(a) indicates the differences between the inviscid solutions obtained using a fine grid and a coarse grid. Here the marching steps are taken to be 1% of the cone length. The coarse grid contains 140 points in the normal direction, whereas the fine grid contains 340 points. For a grid of 340 normal points, the marching step was varied from 1% of the cone length to 2%; the effects of the marching step size on the solution are shown in Fig. 6. The bow-shock is well captured on the coarse grid, but in order to resolve the tail shock/expansion fan interaction, more grid points are needed. This test case is very challenging for the marching code, since the small freestream Mach number and small cone angle results in very weak shocks, and a weak expansion fan.

Viscous calculations were also performed with the fine grid of 340 points in normal direction and a marching step size of

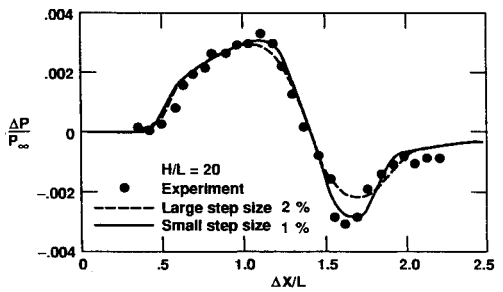

Fig. 6 Comparison of the overpressure signals at 20 cone lengths for different step sizes.

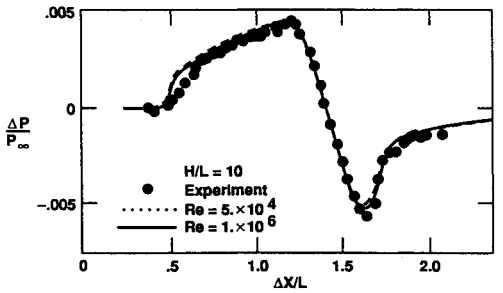

Fig. 7 Effect of Reynolds number on overpressure signals at 10 cone lengths. Model 1, $M_\infty = 1.68$.

1% of the cone length. Overpressure signals at 10 cone lengths with $Re = 5 \times 10^4$ and $Re = 1 \times 10^6$ are presented in Fig. 7. The calculations assumed an adiabatic body surface and a freestream temperature of 275 K. Since the test was run at constant total pressure and the Reynolds number varied due to changing total temperature, the actual Reynolds number associated with the test was not known. It is observed that the presence of the thin, attached boundary-layer does not produce significant differences from the inviscid calculation.

Model 2: Low Aspect Ratio Wing

The second configuration considered was the low-aspect-ratio wing shown in Fig. 8a.[5] The freestream Mach number for the wind-tunnel test was 2.01. A sample computational surface grid is shown in Fig. 8b. The quarter-plane contains 40 points in the circumferential direction and 140 in the radial direction. The overpressure signal was obtained 8 chord lengths below the wing ($H/L = 8$). The calculation was performed at $\alpha = 0$.

Two computational grids were generated, one for the isolated wing (as shown in Fig. 8b), and one with the sting that was present in the wind tunnel experiment. It was found that the overpressure signals from wing-alone and sting-mounted wing calculations had no major differences, even at a short distance $H/L = 1$.

Figure 9a shows the overpressure signals at $H/L = 1$ obtained from viscous (dotted line) and the inviscid (solid line) calculations. Notice that the tail-shock for the viscous calculation is slightly downstream of the inviscid-shock location. Because the PNS assumptions eliminate upstream influence, the presence of a boundary-layer effectively delays the formation of a tail-shock at the wing-trailing edge. Boundary-layer displacement also causes the bow-shock to be slightly upstream of the inviscid prediction.

The inviscid calculation of the overpressure at one body length required 54 min of cpu time on a Cray YMP. Because of the step-size restriction associated with the viscous grid clustering, the viscous calculation required 210 min of cpu time.

The overpressure signals at 1 body length obtained from the viscous and inviscid calculations were used as input to a quasilinear extrapolation code based on the F-function theory. This is approach 2, described in the previous section, that gives the overpressure signatures at 8 body lengths, as

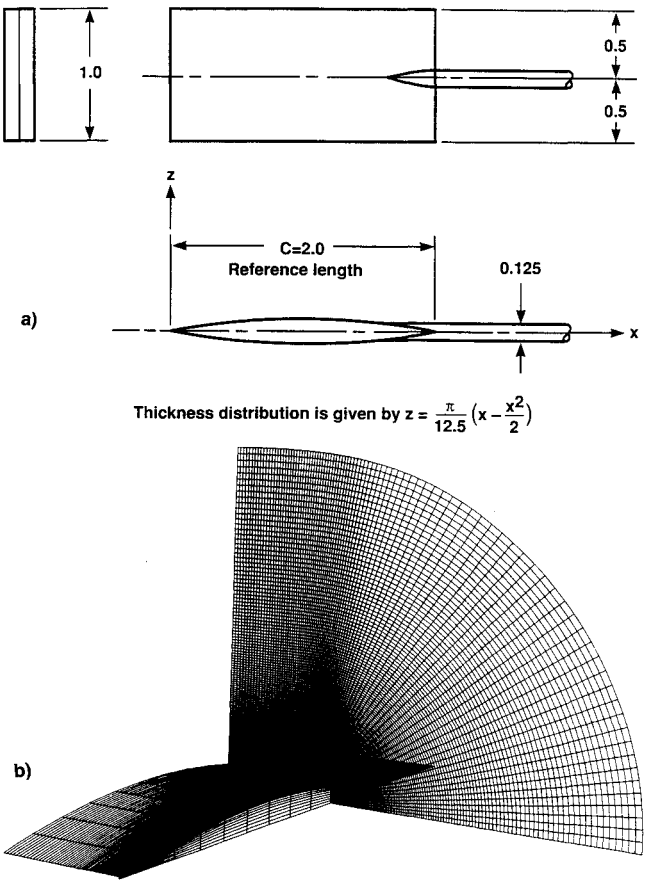

Fig. 8 a) Model 2: Geometry of the low-aspect-ratio wing[5], all dimensions in inches; b) computational grid of the low aspect ratio wing.

shown in Fig. 9b. It is seen that the numerical predictions agree with the wind-tunnel data. The UPSYM calculation at 8 body lengths, also shown in Fig. 9b, predicts the shock points and the peaks accurately, although the gradient of the shock jump is smeared. Inadequate grid resolution near the shock caused excessive dissipation and smearing of the pressure gradient.

Model 3: Delta-Wing Body (Nonlifting Case)

The third configuration considered was the delta-wing body shown in Fig. 10a.[4] The freestream Mach number for the wind-tunnel test was 2.7. The computational grid contained 40 points in the circumferential direction and 140 in the normal direction. Due to quadrilateral symmetry, the computational grid modeled the quarter plane only. Because of the findings in the previous test case, the actual sting thicknes was not modeled. In the computational grid, the sting was as thick as the fuselage. A sample of the computational grid is shown in Fig. 10b. The overpressure signal was obtained at a distance of 3.1 body lengths. Viscous and inviscid near-field solutions were obtained using the UPS3D code for the region from the nose to approximately 1 body length downstream of the trailing edge. The inviscid solution was computed with a step size of 0.06–0.18% of the body length and required about 26 min of cpu time. The viscous solution was obtained using a step-size of 0.018% of the body length and required about 86 min of cpu time on the Cray YMP.

The inviscid solution at the vertical plane of symmetry was used as a starting solution for the UPSYM extrapolation, with 2 lines in the circumferential direction and 400 in the radial direction (this is approach 1). This extrapolation process, using a step-size of 0.01, required about 40 min of cpu time on the Cray YMP to march 10 body lengths downstream to obtain the overpressure signature. This calculation defined all the shock points and captured the bow-shock and the wing-shock,

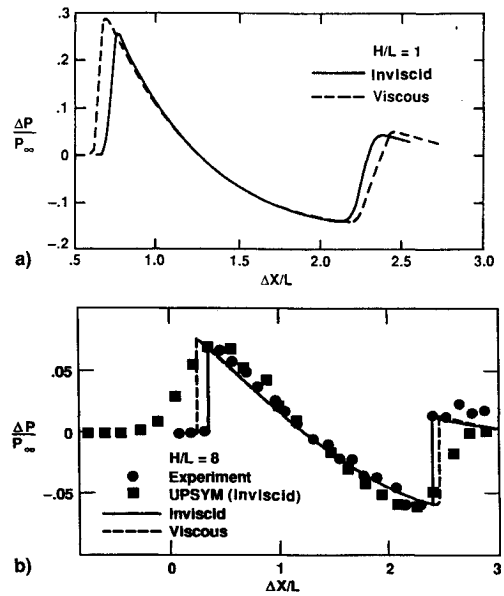

Fig. 9 a) Overpressure signals of viscous and inviscid calculations in the near-field. Model 2, $M = 2.01$. b) Overpressure signal at 8 chord lengths. Overpressure obtained by F-function extrapolation from the signal at one chord length. Model 2, $M_\infty = 2.01$.

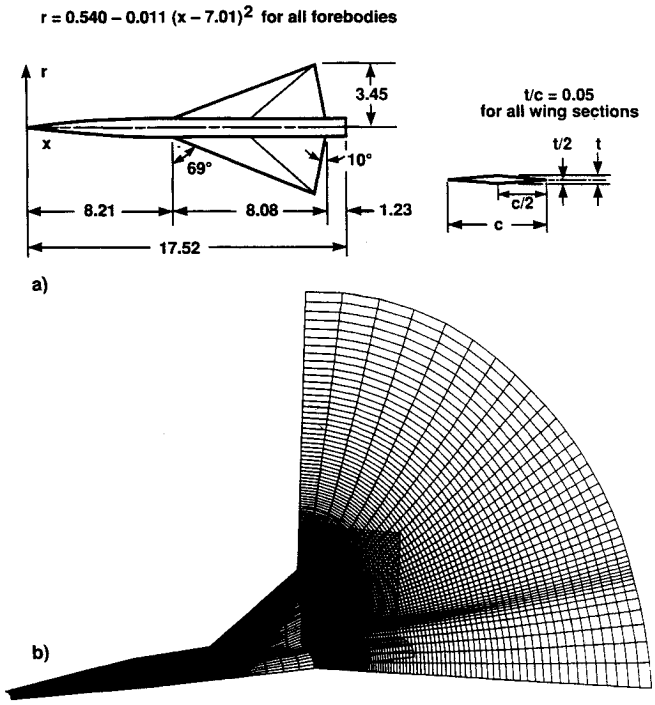

Fig. 10 a) Model 3: Geometry of the delta-wing body[4], all dimensions in inches; b) computational grid of the wing-body with 40 points in the circumferential direction and 140 in the normal direction.

but the tail-shock/expansion fan interaction was poorly resolved, because of a lack of grid points. A series of numerical experiments, as indicated in Fig. 11, showed that increasing the number of grid points improved the prediction of the tail-shock/expansion fan interaction. The solutions did not match well downstream of the tail-shock because the wind-tunnel model's sting thickness was not modeled.

The number of grid points required in these calculations for accurate sonic-boom prediction led to the consideration of an adaptive grid. An adaptive grid has recently been implemented in the UPS3D code with successful results in two-dimensional and axisymmetric calculations.[17] In the present application, adaptive gridding was only utilized for the UP-

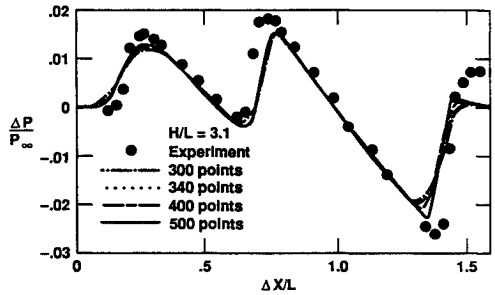

Fig. 11 Comparison of the overpressures of the wing-body with grid refinement in the radial direction. Model 3, $M_\infty = 2.7$, $\alpha = 0$.

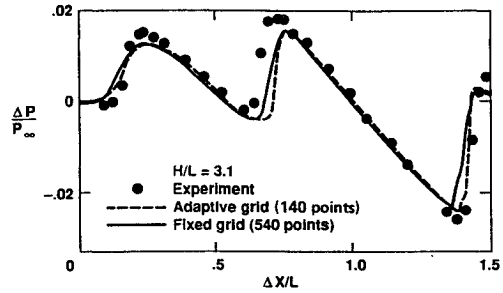

Fig. 12 Effect of grid adaption on inviscid solution. Model 3, $M_\infty = 2.7$, $\alpha = 0$.

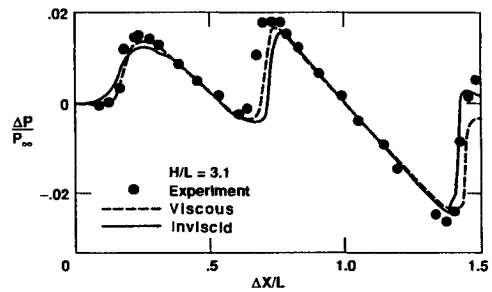

Fig. 13 Overpressures from viscious and inviscid calculations. Model 3, $M_\infty = 2.7$, $\alpha = 0$.

SYM extrapolation and grids were only adapted in the radial direction.

Numerical experiments showed that acceptable results could be obtained from the adaptive grid procedure with 140 radial grid points and a step-size of 0.01. The UPSYM extrapolations of the inviscid and viscous solutions required approximately 24 and 33 min cpu time, respectively. In Fig. 12, the inviscid solution indicates the improved results using adaptive grids. Both the viscous and inviscid solutions from the adaptive grid agree fairly well with the wind-tunnel data as shown in Fig. 13. The differences between the viscous and inviscid solution are similar to those observed in the preceding case: the leading-edge shocks are displaced upstream, and the trailing-edge shocks downstream, by a viscous UPS3D calculation. The improved prediction of the shock-peaks by the viscous solution was primarily due to the smaller spatial marching step-size necessitated by the fine grid. Numerical experiments have shown that an inviscid calculation with a comparable step-size yields essentially the same result.

The overpressure signatures at $H/L = 1$, 1.5, and 2, obtained from the viscous UPS3D calculation and followed by the UPSYM extrapolation, were used as inputs to the quasilinear extrapolation code. This procedure combines approach 1 and 2, and the results at 3.1 body lengths are shown in Fig. 14. The result obtained by approach 1 is also shown in Fig. 14. It is noted that an acceptable result can be obtained by extrapolating the CFD solution from as near as 1 body length. Thus, CFD can provide a near-field flow solution for an F-function extrapolation code based on the F-function theory.

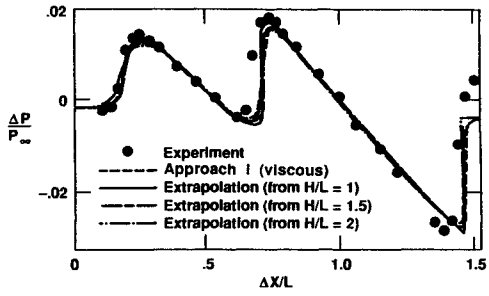

Fig. 14 Overpressure signal at 3.1 body lengths (H/L = 3.1) extrapolated from near field altitudes. Model 3, M_∞ = 2.7, α = 0.

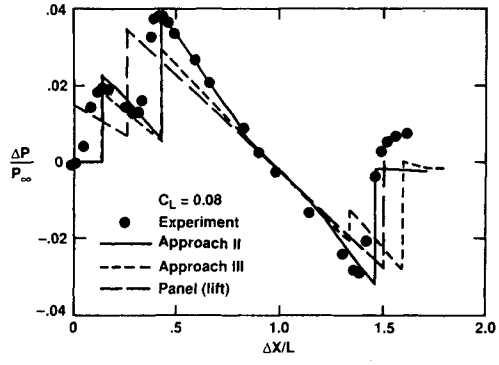

Fig. 15 Overpressure signal at 3.1 body lengths (H/L = 3.1) with C_L = 0.08. Model 3, M_∞ = 2.7, α = 3.3.

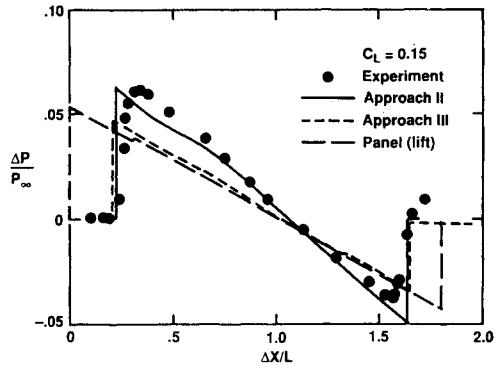

Fig. 16 Overpressure signal at 3.1 body lengths (H/L = 3.1) with C_L = 0.15. Model 3, M_∞ = 2.7, α = 6.4.

Delta-Wing Body (Lifting Case)

For calculations with lift, the computational grid modeled the half-plane that contained 83 points in the circumferential direction and 140 in the normal direction. It was found that for lifting cases, the sting at the back of the wind-tunnel model did affect the sonic boom. A new grid was generated so that the physical sting, whose diameter was 0.15 unit, was modeled.

Figures 15 and 16 show the results obtained by the theory based on the total equivalent area distribution (Eqs. (1–3)) using a panel method[18] and CFD (approach 3) for the lift contribution. The panel method results were produced in Ref. 4. It is noticed that, although the shock-peaks were underpredicted by approach 3, they are well-located. The overpressure signals at H/L = 0.6 obtained from the inviscid UPS3D calculation were used as inputs to the F-function extrapolation code. Figures 15 and 16 indicate that approach 2 outperforms the methods based solely on equivalent area distribution.

We now consider how the sting of the wind-tunnel model affects the sonic boom measurement. For the case of M_∞ = 1.68 and C_L = 0.08, Fig. 17 indicates that a calculation with the grid containing the physical sting (solid line) agrees with the wind-tunnel data, whereas the result from the old grid

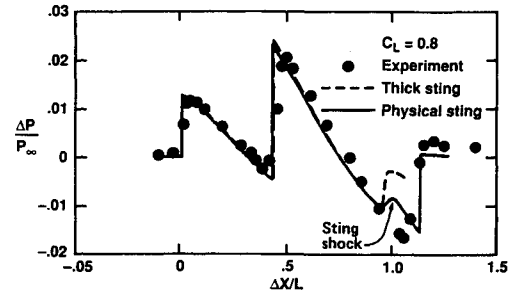

Fig. 17 Effect of wind-tunnel sting on overpressure at 3.6 body lengths (H/L = 3.6). Model 3, M_∞ = 1.68.

(dash line) has a shorter expansion. The extended expansion is due to the "step" between the sting and the fuselage. This observation suggests that an exhaust plume with increased blockage, analogous to the thick sting, could reduce the sonic boom. The wind-tunnel data in Fig. 17 does not show the sting-shock as clearly as the CFD result (solid line). In the wind-tunnel, both the model and the probe vibrate during the experiment, and the wind-tunnel data was the average of a large number of measurements. The disappearance of the sting-shock in the wind-tunnel data may be due to the averaging and/or the coarse experimental data.[19]

Concluding Remarks

Accurate sonic-boom prediction is needed in the development of next-generation supersonic transports. Existing theories based on equivalent area distribution and panel methods cannot provide sufficient accuracy. This study has demonstrated that CFD can provide near-field flow solutions accurate enough to be used for sonic-boom prediction. The three approaches have demonstrated the efficiency and accuracy of the acoustic propagation techniques. The results have shown that CFD can combine with the F-function extrapolation method to propagate the pressure disturbances to the mid-field and provide accurate answers. Thus, CFD can be used as a tool in the iterative loop of the low-boom aircraft design. While this is computationally expensive compared to techniques based on the linear theory, the approach is more versatile and may prove useful when more detailed information is needed.

The results in this paper show that for lifting cases, the sting of the wind-tunnel model affects the structure of sonic boom. The demonstrated interference of the sting suggests that the interference of the exhaust plume may also be important.

The thin, attached boundary layer for these cases had a negligible effect on the mid- and far-field pressure signature. However, the improved grid resolution required to obtain viscous solutions demonstrated the sensitivity of the mid-field signature to the shock and expansion resolution near the body. To alleviate the computational expense of extremely fine grids, a solution-adaptive grid procedure was implemented which produced accurate solutions with one-third as many grid points.

References

[1]Rao, P. S., "Supersonic Bangs," *Aeronautical Quarterly*, Vol. 7, Pt. 1, 1956, pp. 21–44 and Vol.7, Pt. 2, 1956, pp. 135–155.

[2]Lansing, D. L., "Application of Acoustic Theory to Prediction of Sonic-Boom Patterns from Maneuvering Aircraft," NASA TN D-1860, 1964.

[3]McLean, F. G., "Some Nonasymptotic Effects of the Sonic Boom of Large Airplanes," NASA TN D-2877, 1965.

[4]Hunton, L., Hicks, R., and Mendoza, J., "Some Effects of Wing Planform on Sonic Boom," NASA TN D-7160, 1973.

[5]Mendoza, J., and Hicks, R., "Further Studies of The Extrapolation of Near-Field Overpressure Data," NASA TM X-2219, 1971.

[6]Whitham, G. B., "The Flow Pattern of a Supersonic Projectile," *Communications on Pure and Applied Mathematics*, Vol. 5, No. 3, 1952, pp. 301–348.

[7]Lighthill, M. J., *General Theory of High Speed Aerodynamics*, Sec. E; see also *High Speed Aerodynamics and Propulsion*, Vol. 6, Princeton Univ. Press, Princeton, NJ, 1954, pp. 345–389.

[8]Walkden, F., "The Shock Pattern of a Wing-Body Combination, Far From the Flight Path," *Aeronautical Quarterly*, Vol. 9, Pt. 2, May 1958, pp. 164–194.

[9]Seebass, R., and George, A., "Sonic Boom Minimization," *Journal of Acoustical Society of America*, Vol. 51, No. 2, Pt. 3, 1972.

[10]Darden, C., "Sonic-Boom Minimization With Nose-Bluntness Relaxation," NASA TP-1348, 1979.

[11]Mack, R., and Darden, C., "Wind-Tunnel Investigation of the Validity of a Sonic-Boom-Minimization Concept," NASA TP-1421, 1979.

[12]Morris, C., Winston, M., and Morris, S., Jr., "Some Key Considerations for High-Speed Civil Transports," AIAA Paper 88-4466, Sept. 1988.

[13]Lawrence, S., Chaussee, D., and Tannehill, J., "Application of an Upwind Algorithm to the 3-D Parabolized Navier-Stokes Equations," AIAA Paper 87-1112, June 1987.

[14]Roe, P. L., "Approximate Reimann Solvers, Parameter Vectors, and Difference Schemes," *Journal of Computational Physics*, Vol. 43, 1981, pp. 357–372.

[15]Lockman, W. K., Lawrence, S. L., and Cleary, J. W., "Flow over an All-Body Hypersonic Aircraft: Experiment and Computation," *Journal of Spacecraft and Rockets*, Vol. 29, No. 1, 1992, pp. 7–15.

[16]Hicks, R., and Mendoza, J., "Prediction of Aircraft Sonic Boom Characteristics from Experimental Near Field Results," NASA TM X1477, Nov. 1967.

[17]Harvey, A., Acharya, S., Lawrence, S., and Cheung, S. "Solution Adaptive Grid Procedure for an Upwinded Parabolized Flow Solver," AIAA Paper 90-1567, June 1990.

[18]Carmichal, R., Castellano, C., and Chen, C., "The use of Finite Element Methods for Predicting the Aerodynamics of Wing-Body Combinations. Analytic Methods in Aircraft Aerodynamics," NASA SP-228, 1970.

[19]Mendoza, J., private communication, May 1990.